Complex-scaled relativistic configuration-interaction study of the *LL* resonances in heliumlike ions: From boron to argon

V. A. Zaytsev, I. A. Maltsev, I. I. Tupitsyn, and V. M. Shabaev
Department of Physics, St. Petersburg State University, Universitetskaya Naberezhnaya 7/9, 199034 St. Petersburg, Russia

(Received 26 September 2019; published 13 November 2019)

Energies and Auger widths of the *LL* resonances in He-like ions from boron to argon are evaluated by means of a complex-scaled configuration-interaction approach within the framework of the Dirac-Coulomb-Breit Hamiltonian. The nuclear recoil and QED corrections are also taken into account. The results obtained are compared with other calculations based on the complex-scaling method as well as with the related results evaluated by using the stabilization and basis balancing methods.

DOI: 10.1103/PhysRevA.100.052504

I. INTRODUCTION

Autoionizing states of atomic or ionic systems are the excited states which can decay due to the electron-electron interactions via emission of one (or more) electrons. A special place among such states is held by the first autoionizing states of He-like systems; namely, levels of the *LL* resonance groups. The simplicity of these systems makes them attractive for both theoretical and experimental investigations. The investigations aimed at determining the energies of these levels are of particular interest for plasma diagnostics [1–4] and cosmological [5] and fusion research (see, e.g., the review [6]). A new interest in studying the characteristics of the *LL* resonances was caused by a recent experiment [7]. In this experiment, a new level of accuracy for the energy of the autoionizing states of the He-like carbon ion was reached. Experimental data of such accuracy being complemented by the theoretical predictions of the same precision allow one to set these states as energy-reference standards at synchrotron radiation facilities. The precise theoretical predictions for the energies of the *LL* resonances are, therefore, highly demanded.

For the accurate evaluation of the energies of autoionizing states, which are strongly affected by electron correlations, the high-precision many-electron methods such as coupled cluster and configuration interaction are required. These methods, although successfully applied for the calculations of bound-level energies, fail when naively applied for the description of resonances. The energies of such resonances show a strong dependence on the parameters of the basis set, e.g., the convergence of the resonance energy with respect to the number of basis functions, which is one of the basis-set parameters, is very weak or even absent. This is explained by the fact that the autoionizing states are embedded into the positive-energy continuum. As a result, they cannot be described by square-integrable functions which form the basis set of the coupled-cluster and configuration-interaction methods. This problem can be naturally solved with the usage of the complex-scaling approach which is based on the analytical properties of the spectrum of a Hamiltonian being dilated into the complex plane. The first mathematical analysis of these properties was reported in Refs. [8,9] for the nonrelativistic Hamiltonian and in Refs. [10–12] for the relativistic one. In these works, it was shown that in the spectra of the dilated Hamiltonian the autoionizing states are separated from the continuum. The wave functions of these states, therefore, become square integrable and can be investigated with conventional many-electron methods. That makes the complex-scaling approach a powerful tool for studying properties of resonances appearing in various systems and processes. As examples, the resonances of nuclei [13–16], few-electron systems [17–23], and molecules [24,25] were investigated by using this method. More applications, as well as the details of the complex-scaling approach, can be found in the reviews [26–31]. It is also worth noting that the dilated Hamiltonian is not a Hermitian but a symmetric operator with complex eigenvalues. The real and imaginary parts of the eigenvalues corresponding to the autoionizing states give the energies and Auger widths of the states, respectively.

Apart from the complex-scaling approach, one can apply the stabilization or basis balancing methods. The stabilization method (SM) was pioneered by Holøien and Midtdal [32] and utilized in numerous investigations [33–37]. The basis balancing method (BBM) was worked out by Yerokhin with co-authors just recently [38] and was applied for the calculation of the energies of the autoionizing levels of Li-like ions in a wide range of the nuclear charge number [39]. Both methods are applied to the conventional Hermitian Hamiltonian and, as a result, only the real arithmetic is involved that provides a considerable computational advantage. However, the energy of the autoionizing state obtained within SM or BBM can differ from the exact energy by a shift arising due to the inappropriate treatment of the interaction with the continuum. The advantages of these methods over the complex-scaling approach, thus, can be completely lost in some cases. In view of the considerable progress in experimental accuracy for the energies of the autoionizing states [7], the revision of the applicability of the SM and BBM is required.

In the present paper, we apply the configuration interaction (CI) coupled with the complex-scaling (CS) approach to solve

the Dirac-Coulomb-Breit (DCB) equation for LL resonances of He-like ions in the range from boron to argon. The configuration space is spanned by the one-electron Dirac orbitals being constructed from the B splines. The DCB energies are supplemented with the quantum electrodynamics (QED), nuclear recoil, and frequency-dependent Breit corrections. We also estimate the difference of the energies obtained within the SM and BBM with ones calculated employing the complex-scaling approach. In case of the $2s^2$ level of the He-like carbon ion, it is found that the energy difference between these three methods exceeds the uncertainty reached in the recent experiment [7].

In the paper, for theoretical expressions the Heaviside charge unit ($e^2 = 4\pi\alpha c$) and $\hbar = 1$ are used meanwhile numerical results are presented in atomic units ($m_e = \hbar = e{=}1$).

II. BASIC FORMALISM

We start with the formulation of the basic principles of the configuration-interaction with the complex-scaling approach for the solution of the few-electron DCB equation (for a detailed description see, e.g., the review [30]). Here we consider the simplest variant of the CS; namely, the uniform complex rotation. In this case, the radial variable r is transformed as

$$r \to re^{i\theta}, \tag{1}$$

with θ being a constant rotation angle. This transformation leads to the following complex rotated DCB Hamiltonian:

$$H^{(\theta)}_{\rm DCB} = \sum_j h^{(\theta)}_D(j) + e^{-i\theta}\sum_{j<k}[V_C(j,k) + V_B(j,k)],$$
$$j,k = 1,\ldots,N. \tag{2}$$

Here N stands for the total number of the electrons and $h^{(\theta)}_D$ is the scaled one-electron Dirac Hamiltonian given by

$$h^{(\theta)}_D(j) = e^{-i\theta}c\boldsymbol{\alpha}_j\cdot\mathbf{p}_j + (\beta_j - 1)m_ec^2 + V_{\rm nuc}(r_je^{i\theta}), \tag{3}$$

where $\boldsymbol{\alpha}$ and β are the Dirac matrices, $\mathbf{p}$ is the momentum operator, and $V_{\rm nuc}$ is the nuclear potential. In the present paper, we use the uniformly charged sphere model for the nuclear charge-density distribution in order to construct the electrostatic nuclear potential [40]. After the dilatation into the complex plane it takes the following form:

$$V_{\rm nuc}(re^{i\theta}) = \begin{cases} -\frac{\alpha Zc}{2R_{\rm nuc}}\left(3 - e^{2i\theta}\frac{r^2}{R^2_{\rm nuc}}\right), & r < R_{\rm nuc} \\ -e^{-i\theta}\frac{\alpha Zc}{r}, & r > R_{\rm nuc}. \end{cases} \tag{4}$$

In accordance with Eq. (2) the Coulomb and Breit interelectronic-interaction operators are given by

$$V_C(j,k) = \frac{\alpha c}{r_{jk}}, \tag{5}$$

$$V_B(j,k) = \alpha c\left\{\frac{e^{2i\theta}}{2c^2}\left[h^{(\theta)}_D(j),\left[h^{(\theta)}_D(k), r_{jk}\right]\right] - \frac{\boldsymbol{\alpha}_j\cdot\boldsymbol{\alpha}_k}{r_{jk}}\right\} \tag{6}$$

$$= -\frac{\alpha c}{2r_{jk}}[\boldsymbol{\alpha}_j\cdot\boldsymbol{\alpha}_k + (\boldsymbol{\alpha}_j\cdot\hat{\mathbf{r}}_{jk})(\boldsymbol{\alpha}_k\cdot\hat{\mathbf{r}}_{jk})], \tag{7}$$

respectively. In Eqs. (5) and (7), $\hat{\mathbf{r}}_{jk} = \mathbf{r}_{jk}/r_{jk}$ with $\mathbf{r}_{jk} = \mathbf{r}_j - \mathbf{r}_k$ and $r_{jk} = |\mathbf{r}_{jk}|$. Having performed the complex rotation of the DCB Hamiltonian (2) we now proceed to the construction of its eigenfunctions.

As in the conventional CI method [41,42], the N-electron eigenfunction $\Psi(PJM)$ with the parity P, total angular momentum J, and its projection M is expressed as a linear superposition of the configuration-state functions (CSFs) $\Phi(\gamma_rPJM)$:

$$\Psi(PJM) = \sum_{r=1}^{N_{\rm CSF}} c_r\Phi(\gamma_rPJM), \tag{8}$$

where γ_r stands for all additional quantum numbers which determine uniquely the CSF. The CSFs are eigenstates of the total angular-momentum operators J^2 and J_z, constructed from antisymmetrized products of one-electron Dirac orbitals. Here these orbitals are chosen to be the eigenfunctions of the scaled one-electron Dirac Hamiltonian (3) of the form

$$\psi^{(\theta)}_{\kappa m}(\mathbf{r}) = \frac{e^{-i\theta}}{r}\begin{pmatrix} G^{(\theta)}_\kappa(r)\Omega_{\kappa m}(\hat{\mathbf{r}}) \\ iF^{(\theta)}_\kappa(r)\Omega_{-\kappa m}(\hat{\mathbf{r}}) \end{pmatrix},$$

where $\kappa = (-1)^{l+j+1/2}(j+1/2)$ is the Dirac quantum number determined by the angular momentum j and the parity l, and $\Omega_{\kappa m}$ is the spinor spherical harmonic [43]. As usual in accordance with the basic principles of the relativistic theory with the DCB approximation, the CSFs are constructed only from positive-energy one-electron Dirac orbitals.

As already mentioned, autoionizing levels after the complex scaling are described by the square-integrable and localized wave functions. To good accuracy these wave functions can be represented by the corresponding solutions of the scaled DCB equation in a spherical cavity of finite radius. For the solution of this equation, the CI method with the CSFs constructed from the one-electron Dirac orbitals is utilized. In the present paper, these orbitals are obtained by solving the one-electron Dirac equation within the dual-kinetic-balance finite basis set approach [44] with the basis functions constructed from B splines [45,46]:

$$\begin{pmatrix} G^{(\theta)}_\kappa(r) \\ F^{(\theta)}_\kappa(r) \end{pmatrix} = \sum_{i=1}^{N} C^{(\theta)}_{\kappa,i}\begin{pmatrix} B_i(r) \\ \frac{e^{-i\theta}}{2m_ec}\left[\frac{d}{dr} + \frac{\kappa}{r}\right]B_i(r) \end{pmatrix}$$
$$+ \sum_{i=N+1}^{2N} C^{(\theta)}_{\kappa,i}\begin{pmatrix} \frac{e^{-i\theta}}{2m_ec}\left[\frac{d}{dr} - \frac{\kappa}{r}\right]B_{i-N}(r) \\ B_{i-N}(r) \end{pmatrix}. \tag{9}$$

Within the framework of this method, the spectrum of the one-electron Dirac Hamiltonian including positive (and negative) continuum states is represented by a finite number of the quasistates. The interaction of the resonance with the continuum is, thus, incorporated via the inclusion of the interaction with these quasibound and quasicontinuum states. The resulting scaled DCB Hamiltonian is represented by the symmetric matrix with complex eigenvalues $E - i\Gamma_{\rm Aug}/2$ where E and $\Gamma_{\rm Aug}$ are the energies and Auger widths of the corresponding resonances, respectively.

III. RESULTS AND DISCUSSIONS

A. Comparison of the stabilization and basis balancing methods with the complex-scaling approach

Let us start with a brief description of the principles of the stabilization and basis balancing methods, which are applied to the conventional (Hermitian) Hamiltonian. In the SM [32], the basis-set parameters are chosen in such a way as to provide a minimal value for the rate of change of the energy with respect to a variation of these parameters. Another approach, which consists of manipulating the basis to place the resonance just in the middle between the closest quasicontinuum states in the energy scale, is called the basis balancing method (BBM) [38]. Both these methods utilize the advantages of the finite basis set constructed from the square-integrable functions. As already was mentioned, such basis set functions cannot properly describe the contribution of the continuum to the autoionizing states. That is expressed in the energy shift of the state from the exact value. The size of this shift is, however, strongly resonance dependent and may be negligible in some cases. Here we estimate the difference between the results of the complex-scaling approach with results from the stabilization and basis balancing methods considering the state which is known to be significantly coupled with the continuum; namely, the $2s^2$ autoionizing state of the He-like carbon ion ($Z = 6$). For this purpose, we choose the radial grid, which uniquely defines the basis functions constructed from the B splines, as in Ref. [38]:

$$t_i = t_0 e^{A(i/N)^\gamma}, \tag{10}$$

where $A = \ln(t_{\max}/t_0)$, $t_{\max}$ is the radial size of the spherical cavity, t_0 is the radius of the nucleus, and γ is the basis set parameter. The energies of the autoionizing and quasicontinuum states depend strongly on the parameter γ and form γ-parametric trajectories, which are analyzed in accordance with the SM and BBM. For the sake of simplicity, we include only the CSFs being constructed from one-electron s and p Dirac orbitals. Figure 1 presents the γ-parametric energy trajectories for the $2s^2$ state of the He-like carbon ($Z = 6$) ion obtained in the basis of 30 B splines. This figure also presents the energies obtained with the use of the SM and BBM for each γ-parametric trajectory. From Fig. 1, it is seen that, at γ less than 0.5, the results of the SM and BBM are very close to each other. We note that the most accurate results are expected at small γ for which the density of the quasicontinuum states in the vicinity of resonance is sufficiently high. On the other hand, the states have to be well separated from one another to allow clear identification of the autoionizing state. In our case, both of these requirements are fulfilled for γ from 0.3 to 0.5. Before we proceed to the investigation of the convergence with respect to the number of B splines, let us explore how the results obtained within the CS approach depend on the γ parameter.

As was discussed in the preceding section, in the uniform complex rotation approach, the Hamiltonian depends on the θ parameter. Energies of the bound and quasibound states in this method are, however, θ independent for $\theta_c < \theta < \pi/2$, where θ_c is the critical angle, which can be approximately evaluated

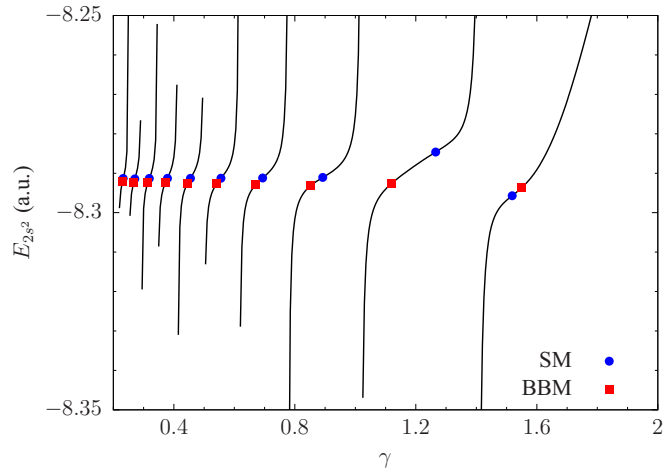

FIG. 1. Energy of the $2s^2$ state of the He-like carbon ($Z = 6$) ion as a function of the parameter γ [see Eq. (10)]. The CSFs are constructed from one-electron s and p Dirac orbitals obtained in the basis of 30 B splines. The size of the spherical box was chosen to be 15 a.u. Blue circles and red squares correspond to the γ parameters chosen in accordance with the stabilization and basis balancing methods, respectively.

with the use of the nonrelativistic expression [8,47]

$$\theta_c = \tfrac{1}{2}\arctan\left\{\Gamma_{\mathrm{Aug}}/[2(E - E_t)]\right\}. \tag{11}$$

Here Γ_{Aug} and E are the Auger width and the energy of the level of interest, respectively, and E_t is the autoionization threshold energy, which for the $2s^2$ state is provided by the ground state of the corresponding H-like ion. Note that the energies do not depend on θ only if the complete or large basis set is utilized. In practice, however, one has to deal with an incomplete basis set that requires a search of an optimal angle for the uniform complex rotation. Although this angle should be larger than θ_c, we start the search from zero degrees. The optimal angle corresponds to the stationary point of the θ-parametric energy curve in the complex plane. In our case,

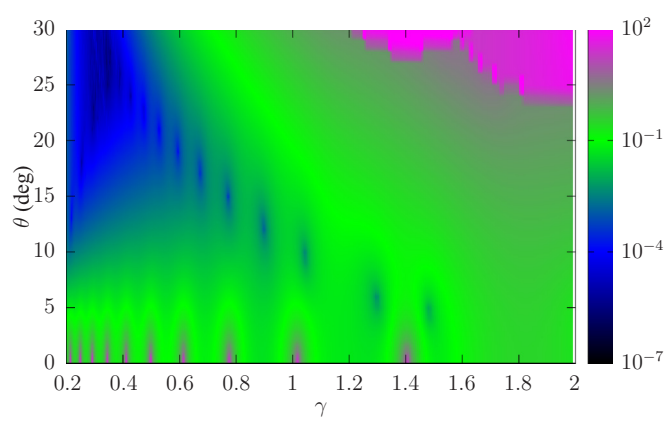

FIG. 2. Dependence of the s function (in a.u.) given by Eq. (12) on the θ and γ parameters for the $2s^2$ state of the He-like carbon ($Z = 6$) ion. The CSFs are constructed from one-electron s and p Dirac orbitals obtained in the basis of 30 B splines. The size of the spherical box was chosen to be 15 a.u.

TABLE I. Energy (in a.u.) of the $2s^2$ state of the He-like C ($Z = 6$) ion obtained within the stabilization method (SM), the basis balancing method (BBM), and the complex-scaling (CS) approach. The CSFs are constructed from one-electron s and p Dirac orbitals obtained in the basis of N functions. The size of the spherical box was chosen to be 15 a.u. Parameter γ is varied in the range between 0.3 and 0.5. The calculations within the CS approach are performed for θ varying from 20° to 25°.

			CS	
N	SM	BBM	Re(E)	Im(E) $\times 10^3$
30	−8.291 30(3)	−8.2924(2)	−8.291 450(4)	−3.529(4)
40	−8.291 34(4)	−8.2921(1)	−8.291 449 9(2)	−3.5290(3)
50	−8.291 37(3)	−8.291 97(3)	−8.291 449 98(9)	−3.529 06(15)
60	−8.291 40(2)	−8.2919(1)	−8.291 449 98(9)	−3.529 07(13)

one needs to find the stationary point of the (γ, θ)-parametric energy surface in the complex plane. That is equivalent to the search for the minimum of the function

$$s(\gamma, \theta) \equiv \sqrt{\left|\frac{dE}{d\theta}\right|^2 + \left|\frac{dE}{d\gamma}\right|^2}. \tag{12}$$

Figure 2 presents the s function (12) for the $2s^2$ state of the He-like carbon ($Z = 6$) ion obtained in the basis of 30 B splines. From this figure it is seen that the $s(\gamma, \theta)$ function takes minimal values at γ from 0.3 to 0.5 and θ from 20° to 30°. For γ and θ changing within this area, the energy of the $2s^2$ state exhibits very stable behavior.

We now turn to the investigation of the convergence of the results obtained within the SM, BBM, and CS methods with respect to the number of basis functions. Table I presents the energy of the $2s^2$ state of the He-like C ($Z = 6$) ion for different numbers of B splines.

The calculations within the stabilization and basis balancing methods are performed for the γ parameter varying from 0.3 to 0.5. In Table I, we present the average values of the energies originating from different energetic curves corresponding to this γ interval (see Fig. 1). The uncertainty reflects the dependence of the results on the choice of the curve. From Table I, it is seen that the BBM results depend more strongly on the energetic curve than do the SM results. This can be due to the fact that, in the BBM, the resonance position is balanced with respect to the closest quasicontinuum states whereas in the SM the whole spectra is effectively taken into account. For both methods, the dependence on the energetic curve strongly masks the convergence with respect to the number of basis functions and gives the main source of the uncertainty. The calculations within the CS approach are performed for γ varying from 0.3 to 0.5 and θ varying in the range between 20° and 25°. The dependence of the energy on the γ and θ parameters forms the uncertainty indicated in Table I. It is seen that the energy obtained within the CS approach exhibits extremely fast convergence with respect to the number of basis functions. It is also seen that the energies obtained within the SM and BBM differ from the energy calculated by using the complex-scaling approach by more than 1 and 10 meV, respectively, the values which actually define accuracy limits of the SM and BBM. We note also that, working with SM and BBM, one needs to reselect the basis set parameters each time when the number of basis functions is enlarged. The necessity of this procedure drastically increases the required computation time and, thus, strongly reduces the advantage of the real arithmetic.

B. Energies and Auger widths of the *LL* resonances

We now apply the configuration-interaction complex-scaling method for the calculation of the energies and Auger width of LL resonances of the He-like ions from boron ($Z = 5$) to argon ($Z = 18$). The simplicity of the system studied allows performing the full CI calculations, i.e., the configuration space is formed from all possible combinations of the one-electron Dirac orbitals appearing for a given number of B splines. In the present paper, B splines of order 11 are utilized. Such a high order of B splines is chosen to guarantee the correct behavior of the one-electron Dirac orbitals with orbital angular momenta up to $L = 8$ at the origin. The one-electron orbitals with proper behavior at the origin appear to be less

TABLE II. Energy E and Auger width $\Gamma_{\rm Aug}$ of the $2s^2$ state of the He-like carbon ($Z = 6$) ion obtained within the configuration-interaction complex-scaling method. The CSFs are constructed from one-electron Dirac orbitals with orbital angular momenta up to $L_{\rm max}$ being obtained in the basis of N B splines. The size of the spherical box was chosen to be 15 a.u., $\gamma = 0.3$, and $\theta = 20°$. The values listed after the second row are the increments obtained by successively adding configurations while increasing $L_{\rm max}$.

	E [a.u.]			$\Gamma_{\rm Aug} \times 10^3$ [a.u.]		
$L_{\rm max}$	$N = 30$	$N = 40$	$N = 50$	$N = 30$	$N = 40$	$N = 50$
1	−8.291 450 6	−8.291 450 0	−8.291 449 9	7.056 59	7.058 01	7.058 00
2	−0.000 796 1	−0.000 796 0	−0.000 796 0	−0.081 75	−0.081 55	−0.081 52
3	−0.000 118 0	−0.000 118 3	−0.000 118 3	−0.018 88	−0.018 72	−0.018 70
4	−0.000 037 5	−0.000 037 8	−0.000 037 8	−0.006 72	−0.006 58	−0.006 56
5	−0.000 015 9	−0.000 016 1	−0.000 016 2	−0.003 02	−0.002 91	−0.002 89
6	−0.000 007 8	−0.000 008 1	−0.000 008 1	−0.001 57	−0.001 49	−0.001 48
7	−0.000 004 3	−0.000 004 5	−0.000 004 5	−0.000 91	−0.000 85	−0.000 83
8	−0.000 002 5	−0.000 002 7	−0.000 002 7	−0.000 57	−0.000 52	−0.000 51
9–∞	−0.000 005 7	−0.000 006 8	−0.000 007 1	−0.001 76	−0.001 49	−0.001 42
Total	−8.292 438 3	−8.292 440 2	−8.292 440 7	6.941 41	6.943 91	6.944 07

TABLE III. Energies $E_{\rm tot}$ and Auger widths $\Gamma_{\rm Aug}$ of the LL resonances of the He-like ions from boron ($Z = 5$) to argon ($Z = 18$), in a.u. The CS DCB energy, the QED correction, and the nuclear recoil correction are explicitly shown. Energies $E_{\rm tot}$ are supplemented with the total uncertainties from all calculated and uncalculated contributions. The nuclear charge radii are taken from Ref. [59].

Ion	Resonance	J	DCB	Recoil	QED	$E_{\rm tot}$	$\Gamma_{\rm Aug}$
$^{11}B^{3+}$	$2s_{1/2}^2$	0	−5.662 877 1	0.000 282 1	0.000 085 6	−5.662 509(24)	$6.674(1) \times 10^{-3}$
	$2p_{1/2}^2$	0	−5.470 235 0	0.000 280 5	−0.000 000 7	−5.469 955 2(88)	$<10^{-6}$
	$2p_{3/2}^2$	0	−5.145 761 9	0.000 276 0	0.000 020 3	−5.145 466(42)	$3.0(2) \times 10^{-4}$
		2	−5.469 436 0	0.000 280 4	0.000 001 3	−5.469 154 3(48)	$<2 \times 10^{-6}$
	$2s_{1/2}2p_{1/2}$	0	−5.615 179 4	0.000 281 1	0.000 054 1	−5.614 844(13)	$3.314(7) \times 10^{-4}$
		1	−5.614 917 3	0.000 281 1	0.000 054 8	−5.614 582(13)	$3.277(7) \times 10^{-4}$
	$2s_{1/2}2p_{3/2}$	1	−5.381 734 4	0.000 271 0	0.000 046 5	−5.381 417(54)	$3.09(4) \times 10^{-3}$
		2	−5.614 327 8	0.000 281 0	0.000 056 2	−5.613 991(13)	$3.241(5) \times 10^{-4}$
	$2p_{1/2}2p_{3/2}$	1	−5.469 940 8	0.000 280 5	0.0	−5.469 660 4(36)	$<10^{-6}$
		2	−5.404 473 3	0.000 271 1	0.000 001 8	−5.404 200(30)	$5.52(1) \times 10^{-3}$
$^{12}C^{4+}$	$2s_{1/2}^2$	0	−8.292 440 7	0.000 378 6	0.000 167 9	−8.291 894(41)	$6.944(1) \times 10^{-3}$
	$2p_{1/2}^2$	0	−8.057 969 3	0.000 377 0	−0.000 001 5	−8.057 594(13)	$<2 \times 10^{-7}$
	$2p_{3/2}^2$	0	−7.653 533 8	0.000 372 4	0.000 041 3	−7.653 120(54)	$3.1(1) \times 10^{-4}$
		2	−8.056 242 6	0.000 377 0	0.000 002 8	−8.055 862 8(66)	$6.9(9) \times 10^{-7}$
	$2s_{1/2}2p_{1/2}$	0	−8.234 968 6	0.000 377 7	0.000 105 8	−8.234 485(22)	$3.377(6) \times 10^{-4}$
		1	−8.234 399 8	0.000 377 6	0.000 107 2	−8.233 915(22)	$3.32(1) \times 10^{-4}$
	$2s_{1/2}2p_{3/2}$	1	−7.943 567 5	0.000 366 1	0.000 094 0	−7.943 107(71)	$3.35(4) \times 10^{-3}$
		2	−8.233 140 3	0.000 377 6	0.000 110 2	−8.232 653(22)	$3.27(1) \times 10^{-4}$
	$2p_{1/2}2p_{3/2}$	1	−8.057 340 5	0.000 377 0	0.0	−8.056 963 5(38)	$<10^{-6}$
		2	−7.971 252 5	0.000 366 7	0.000 003 1	−7.970 883(40)	$6.017(9) \times 10^{-3}$
$^{14}N^{5+}$	$2s_{1/2}^2$	0	−11.423 448 0	0.000 447 0	0.000 295 3	−11.42 270 6(64)	$7.146(1) \times 10^{-3}$
	$2p_{1/2}^2$	0	−11.146 890 5	0.000 445 6	−0.000 002 7	−11.146 448(19)	$1.1(6) \times 10^{-7}$
	$2p_{3/2}^2$	0	−10.662 027 6	0.000 441 2	0.000 074 5	−10.661 512(64)	$3.3(2) \times 10^{-4}$
		2	−11.143 596 4	0.000 445 5	0.000 005 4	−11.143 145 5(93)	$1.8(6) \times 10^{-6}$
	$2s_{1/2}2p_{1/2}$	0	−11.356 413 0	0.000 446 2	0.000 185 6	−11.355 781(34)	$3.444(2) \times 10^{-4}$
		1	−11.355 325 6	0.000 446 2	0.000 188 3	−11.354 691(34)	$3.363(6) \times 10^{-4}$
	$2s_{1/2}2p_{3/2}$	1	−11.006 211 3	0.000 434 3	0.000 168 9	−11.005 608(88)	$3.54(4) \times 10^{-3}$
		2	−11.352 940 9	0.000 446 1	0.000 193 9	−11.352 301(34)	$3.289(5) \times 10^{-4}$
	$2p_{1/2}2p_{3/2}$	1	−11.145 698 1	0.000 445 6	0.0	−11.145 252 5(40)	$<10^{-6}$
		2	−11.038 563 4	0.000 435 2	0.000 005 1	−11.038 123(40)	$6.39(2) \times 10^{-3}$
$^{16}O^{6+}$	$2s_{1/2}^2$	0	−15.056 486 6	0.000 515 5	0.000 480 2	−15.055 491(96)	$7.304(1) \times 10^{-3}$
	$2p_{1/2}^2$	0	−14.737 464 3	0.000 514 2	−0.000 004 5	−14.736 955(27)	$2.3(7) \times 10^{-7}$
	$2p_{3/2}^2$	0	−14.171 660 3	0.000 509 9	0.000 123 3	−14.171 027(76)	$3.4(2) \times 10^{-4}$
		2	−14.731 723 8	0.000 514 0	0.000 009 4	−14.731 200(14)	$3.9(3) \times 10^{-6}$
	$2s_{1/2}2p_{1/2}$	0	−14.980 155 6	0.000 514 8	0.000 300 9	−14.979 340(50)	$3.516(5) \times 10^{-4}$
		1	−14.978 259 4	0.000 514 8	0.000 305 6	−14.977 439(50)	$3.409(6) \times 10^{-4}$
	$2s_{1/2}2p_{3/2}$	1	−14.570 258 8	0.000 502 7	0.000 279 0	−14.569 48(11)	$3.69(5) \times 10^{-3}$
		2	−14.974 120 9	0.000 514 6	0.000 315 2	−14.973 291(50)	$3.304(5) \times 10^{-4}$
	$2p_{1/2}2p_{3/2}$	1	−14.735 390 8	0.000 514 1	0.000 000 3	−14.734 876 4(44)	$<10^{-6}$
		2	−14.606 769 5	0.000 503 7	0.000 008 0	−14.606 258(44)	$6.67(3) \times 10^{-3}$
$^{19}F^{7+}$	$2s_{1/2}^2$	0	−19.192 230 3	0.000 553 3	0.000 735 5	−19.190 94(14)	$7.434(3) \times 10^{-3}$
	$2p_{1/2}^2$	0	−18.830 232 1	0.000 552 2	−0.000 006 9	−18.829 687(37)	$4.8(6) \times 10^{-7}$
	$2p_{3/2}^2$	0	−18.182 869 3	0.000 548 2	0.000 191 0	−18.182 130(88)	$3.5(3) \times 10^{-4}$
		2	−18.820 891 7	0.000 551 9	0.000 015 3	−18.820 324(19)	$8(1) \times 10^{-6}$
	$2s_{1/2}2p_{1/2}$	0	−19.106 935 9	0.000 552 8	0.000 459 7	−19.105 923(70)	$3.600(7) \times 10^{-4}$
		1	−19.103 851 9	0.000 552 7	0.000 467 2	−19.102 832(70)	$3.463(7) \times 10^{-4}$
	$2s_{1/2}2p_{3/2}$	1	−18.636 316 1	0.000 541 1	0.000 432 5	−18.635 34(13)	$3.81(4) \times 10^{-3}$
		2	−19.097 127 7	0.000 552 5	0.000 482 8	−19.096 092(70)	$3.326(8) \times 10^{-4}$
	$2p_{1/2}2p_{3/2}$	1	−18.826 854 3	0.000 552 1	0.000 000 7	−18.826 301 5(50)	$<2 \times 10^{-6}$
		2	−18.676 234 3	0.000 542 2	0.000 012 3	−18.675 680(50)	$6.90(4) \times 10^{-3}$
$^{20}Ne^{8+}$	$2s_{1/2}^2$	0	−23.831 447 0	0.000 652 7	0.001 075 2	−23.829 72(19)	$7.542(1) \times 10^{-3}$
	$2p_{1/2}^2$	0	−23.425 814 7	0.000 651 6	−0.000 010 0	−23.425 173(50)	$9.5(4) \times 10^{-7}$
	$2p_{3/2}^2$	0	−22.696 122 6	0.000 647 4	0.000 281 1	−22.695 19(10)	$3.6(2) \times 10^{-4}$
		2	−23.411 414 9	0.000 651 2	0.000 023 5	−23.410 740(28)	$1.47(5) \times 10^{-5}$
	$2s_{1/2}2p_{1/2}$	0	−23.737 593 9	0.000 652 2	0.000 670 1	−23.736 272(96)	$3.690(4) \times 10^{-4}$
		1	−23.732 844 2	0.000 652 1	0.000 681 5	−23.731 511(96)	$3.518(3) \times 10^{-4}$

TABLE III. (*Continued.*)

Ion	Resonance	J	DCB	Recoil	QED	$E_{\rm tot}$	$\Gamma_{\rm Aug}$
	$2s_{1/2}2p_{3/2}$	1	−23.205 029 4	0.000 639 7	0.000 638 1	−23.203 75(16)	$3.91(4) \times 10^{-3}$
		2	−23.722 467 3	0.000 651 8	0.000 705 6	−23.721 110(96)	$3.346(7) \times 10^{-4}$
	$2p_{1/2}2p_{3/2}$	1	−23.420 584 6	0.000 651 4	0.000 001 6	−23.419 931 6(61)	$<2 \times 10^{-6}$
		2	−23.247 336 3	0.000 640 9	0.000 018 6	−23.246 677(59)	$7.08(4) \times 10^{-3}$
$^{13}Na^{9+}$	$2s^2_{1/2}$	0	−28.975 002	0.000 690	0.001 514	−28.972 80(25)	$7.635(1) \times 10^{-3}$
	$2p^2_{1/2}$	0	−28.524 916	0.000 689	−0.000 013	−28.524 240(66)	$1.72(8) \times 10^{-6}$
	$2p^2_{3/2}$	0	−27.711 922	0.000 685	0.000 397	−27.710 84(12)	$3.7(2) \times 10^{-4}$
		2	−28.503 662	0.000 688	0.000 035	−28.502 939(39)	$2.7(1) \times 10^{-5}$
	$2s_{1/2}2p_{1/2}$	0	−28.873 071	0.000 690	0.000 941	−28.871 44(13)	$3.790(5) \times 10^{-4}$
		1	−28.866 072	0.000 690	0.000 957	−28.864 43(13)	$3.581(2) \times 10^{-4}$
	$2s_{1/2}2p_{3/2}$	1	−28.277 097	0.000 677	0.000 905	−28.275 51(20)	$3.99(4) \times 10^{-3}$
		2	−28.850 706	0.000 689	0.000 993	−28.849 02(13)	$3.367(3) \times 10^{-4}$
	$2p_{1/2}2p_{3/2}$	1	−28.517 138	0.000 689	0.000 003	−28.516 446 6(78)	$<2 \times 10^{-6}$
		2	−28.320 470	0.000 679	0.000 028	−28.319 763(70)	$7.23(4) \times 10^{-3}$
$^{24}Mg^{10+}$	$2s^2_{1/2}$	0	−34.623 863	0.000 790	0.002 068	−34.621 01(33)	$7.716(1) \times 10^{-3}$
	$2p^2_{1/2}$	0	−34.128 326	0.000 789	−0.000 017	−34.127 554(85)	$2.91(7) \times 10^{-6}$
	$2p^2_{3/2}$	0	−33.230 798	0.000 785	0.000 542	−33.229 47(14)	$3.9(2) \times 10^{-4}$
		2	−34.098 066	0.000 788	0.000 049	−34.097 229(54)	$4.49(6) \times 10^{-5}$
	$2s_{1/2}2p_{1/2}$	0	−34.514 412	0.000 790	0.001 281	−34.512 34(17)	$3.901(4) \times 10^{-4}$
		1	−34.504 470	0.000 790	0.001 304	−34.502 38(17)	$3.652(5) \times 10^{-4}$
	$2s_{1/2}2p_{3/2}$	1	−33.853 273	0.000 777	0.001 243	−33.851 25(24)	$4.06(4) \times 10^{-3}$
		2	−34.482 472	0.000 789	0.001 355	−34.480 33(17)	$3.387(7) \times 10^{-4}$
	$2p_{1/2}2p_{3/2}$	1	−34.117 134	0.000 789	0.000 005	−34.116 340(10)	$<2 \times 10^{-6}$
		2	−33.896 040	0.000 778	0.000 040	−33.895 222(86)	$7.34(4) \times 10^{-3}$
$^{27}Al^{11+}$	$2s^2_{1/2}$	0	−40.779 109	0.000 827	0.002 752	−40.775 53(42)	$7.788(1) \times 10^{-3}$
	$2p^2_{1/2}$	0	−40.236 929	0.000 826	−0.000 020	−40.236 12(11)	$4.66(6) \times 10^{-6}$
	$2p^2_{3/2}$	0	−39.253 305	0.000 822	0.000 718	−39.251 77(17)	$4.0(2) \times 10^{-4}$
		2	−40.195 135	0.000 825	0.000 067	−40.194 243(72)	$7.4(1) \times 10^{-5}$
	$2s_{1/2}2p_{1/2}$	0	−40.662 765	0.000 827	0.001 699	−40.660 24(21)	$4.025(8) \times 10^{-4}$
		1	−40.649 071	0.000 827	0.001 730	−40.646 51(21)	$3.738(6) \times 10^{-4}$
	$2s_{1/2}2p_{3/2}$	1	−39.934 371	0.000 814	0.001 661	−39.931 90(29)	$4.12(5) \times 10^{-3}$
		2	−40.618 454	0.000 826	0.001 801	−40.615 83(21)	$3.412(7) \times 10^{-4}$
	$2p_{1/2}2p_{3/2}$	1	−40.221 253	0.000 826	0.000 009	−40.220 418(14)	$<2 \times 10^{-6}$
		2	−39.974 458	0.000 816	0.000 058	−39.973 58(10)	$7.42(4) \times 10^{-3}$
$^{28}Si^{12+}$	$2s^2_{1/2}$	0	−47.441 930	0.000 928	0.003 583	−47.437 42(52)	$7.853(1) \times 10^{-3}$
	$2p^2_{1/2}$	0	−46.851 709	0.000 927	−0.000 021	−46.850 80(13)	$7.1(1) \times 10^{-6}$
	$2p^2_{3/2}$	0	−45.780 017	0.000 923	0.000 928	−45.778 17(19)	$4.1(2) \times 10^{-4}$
		2	−46.795 465	0.000 926	0.000 089	−46.794 451(95)	$1.16(1) \times 10^{-4}$
	$2s_{1/2}2p_{1/2}$	0	−47.319 385	0.000 928	0.002 206	−47.316 25(26)	$4.157(2) \times 10^{-4}$
		1	−47.301 016	0.000 928	0.002 247	−47.297 84(26)	$3.84(1) \times 10^{-4}$
	$2s_{1/2}2p_{3/2}$	1	−46.521 263	0.000 914	0.002 171	−46.518 18(34)	$4.17(5) \times 10^{-3}$
		2	−47.259 405	0.000 927	0.002 343	−47.256 14(26)	$3.437(9) \times 10^{-4}$
	$2p_{1/2}2p_{3/2}$	1	−46.830 238	0.000 926	0.000 014	−46.829 298(20)	$6(3) \times 10^{-7}$
		2	−46.556 124	0.000 916	0.000 082	−46.555 13(13)	$7.48(4) \times 10^{-3}$
$^{31}P^{13+}$	$2s^2_{1/2}$	0	−54.613 632	0.000 965	0.004 579	−54.608 09(64)	$7.911(1) \times 10^{-3}$
	$2p^2_{1/2}$	0	−53.973 757	0.000 964	−0.000 017	−53.972 81(16)	$1.05(2) \times 10^{-5}$
	$2p^2_{3/2}$	0	−52.811 508	0.000 959	0.001 175	−52.809 37(22)	$4.3(2) \times 10^{-4}$
		2	−53.899 759	0.000 962	0.000 115	−53.898 68(12)	$1.77(2) \times 10^{-4}$
	$2s_{1/2}2p_{1/2}$	0	−54.485 633	0.000 965	0.002 810	−54.481 86(32)	$4.305(1) \times 10^{-4}$
		1	−54.461 556	0.000 964	0.002 862	−54.457 73(32)	$3.946(7) \times 10^{-4}$
	$2s_{1/2}2p_{3/2}$	1	−53.614 881	0.000 952	0.002 783	−53.611 15(40)	$4.21(5) \times 10^{-3}$
		2	−54.406 141	0.000 963	0.002 991	−54.402 19(32)	$3.47(2) \times 10^{-4}$
	$2p_{1/2}2p_{3/2}$	1	−53.944 897	0.000 963	0.000 021	−53.943 913(28)	$8(4) \times 10^{-7}$
		2	−53.641 418	0.000 953	0.000 114	−53.640 35(17)	$7.50(5) \times 10^{-3}$
$^{32}S^{14+}$	$2s^2_{1/2}$	0	−62.295 647	0.001 066	0.005 757	−62.288 82(78)	$7.963(1) \times 10^{-3}$
	$2p^2_{1/2}$	0	−61.604 283	0.001 065	−0.000 006	−61.603 22(20)	$1.48(2) \times 10^{-5}$
	$2p^2_{3/2}$	0	−60.348 353	0.001 060	0.001 458	−60.345 83(26)	$4.5(2) \times 10^{-4}$
		2	−61.230 680	0.001 063	0.000 144	−61.229 47(21)	$7.48(5) \times 10^{-3}$

TABLE III. (*Continued.*)

Ion	Resonance	J	DCB	Recoil	QED	$E_{\rm tot}$	$\Gamma_{\rm Aug}$
	$2s_{1/2}2p_{1/2}$	0	−62.162 977	0.001 066	0.003 522	−62.158 39(39)	$4.468(1)\times10^{-4}$
		1	−62.132 053	0.001 066	0.003 588	−62.127 40(39)	$4.078(6)\times10^{-4}$
	$2s_{1/2}2p_{3/2}$	1	−61.216 210	0.001 052	0.003 508	−61.211 65(48)	$4.24(5)\times10^{-3}$
		2	−62.059 542	0.001 064	0.003 756	−62.054 72(39)	$3.50(2)\times10^{-4}$
	$2p_{1/2}2p_{3/2}$	1	−61.566 101	0.001 064	0.000 031	−61.565 007(38)	$1.0(3)\times10^{-6}$
		2	−61.508 840	0.001 053	0.000 157	−61.507 63(17)	$2.63(3)\times10^{-4}$
$^{35}Cl^{15+}$	$2s^2_{1/2}$	0	−70.489 528	0.001 103	0.007 135	−70.481 29(94)	$8.012(1)\times10^{-3}$
	$2p^2_{1/2}$	0	−69.744 626	0.001 101	0.000 017	−69.743 51(24)	$2.01(2)\times10^{-5}$
	$2p^2_{3/2}$	0	−68.391 105	0.001 097	0.001 778	−68.388 23(30)	$4.7(2)\times10^{-4}$
		2	−69.324 198	0.001 099	0.000 178	−69.322 92(25)	$7.43(4)\times10^{-3}$
	$2s_{1/2}2p_{1/2}$	0	−70.352 997	0.001 103	0.004 351	−70.347 54(47)	$4.641(1)\times10^{-4}$
		1	−70.313 991	0.001 102	0.004 433	−70.308 46(47)	$4.225(8)\times10^{-4}$
	$2s_{1/2}2p_{3/2}$	1	−69.326 288	0.001 089	0.004 357	−69.320 84(56)	$4.27(6)\times10^{-3}$
		2	−70.220 551	0.001 101	0.004 650	−70.214 80(47)	$3.53(2)\times10^{-4}$
	$2p_{1/2}2p_{3/2}$	1	−69.694 787	0.001 101	0.000 044	−69.693 642(52)	$1.3(8)\times10^{-6}$
		2	−69.623 669	0.001 090	0.000 214	−69.622 36(23)	$3.79(3)\times10^{-4}$
$^{40}Ar^{16+}$	$2s^2_{1/2}$	0	−79.196 961	0.001 084	0.008 730	−79.187 1(11)	$8.056(1)\times10^{-3}$
	$2p^2_{1/2}$	0	−78.396 270	0.001 083	0.000 060	−78.395 13(28)	$2.66(3)\times10^{-5}$
	$2p^2_{3/2}$	0	−76.940 290	0.001 078	0.002 134	−76.937 08(34)	$4.9(3)\times10^{-4}$
		2	−77.922 194	0.001 080	0.000 215	−77.920 90(29)	$7.33(4)\times10^{-3}$
	$2s_{1/2}2p_{1/2}$	0	−79.057 381	0.001 084	0.005 310	−79.050 99(56)	$4.833(1)\times10^{-4}$
		1	−79.008 977	0.001 084	0.005 408	−79.002 49(56)	$4.400(6)\times10^{-4}$
	$2s_{1/2}2p_{3/2}$	1	−77.946 209	0.001 071	0.005 344	−77.939 79(64)	$4.30(6)\times10^{-3}$
		2	−78.890 181	0.001 082	0.005 685	−78.883 41(56)	$3.57(2)\times10^{-4}$
	$2p_{1/2}2p_{3/2}$	1	−78.331 956	0.001 082	0.000 061	−78.330 813(70)	$1.7(7)\times10^{-6}$
		2	−78.245 356	0.001 072	0.000 288	−78.244 00(31)	$5.31(4)\times10^{-4}$

dependent on the choice of the complex rotation angle θ and, thus, provide more accurate results. The accuracy of the DCB eigenvalues, apart from the choice of the θ and γ parameters, depends on the number of B splines and the number of the orbital angular momenta L included. To estimate the uncertainty arising from the number of orbital angular momenta we carry out the CI calculations for $L \leqslant 8$ and estimate the tail contributions via polynomial least square fitting of the increments in powers of $1/L$, as in Refs. [38,48,49]. An example of such an uncertainty analysis is presented in Table II for the $2s^2$ state of the carbon ($Z = 6$) ion. In this table, the results obtained solely for $L_{\rm max} = 0$ are not presented since the inclusion of the p orbitals leads to a drastic change of the energy and Auger width. From Table II, it is seen that, for the basis of more than 40 B splines, the dominant contribution to the uncertainty of the DCB eigenvalues is provided by the configuration states with orbital angular momenta $L \geqslant 9$, whose contributions are taken into account by extrapolation. Therefore, in what follows we solve the complex rotated DCB equation in the configuration space formed from all possible combinations of the one-electron Dirac orbitals constructed out of 40 or 50 B splines.

To obtain the energies of the LL resonances with an accuracy at a few meV level, we supplement the solutions of the complex rotated DCB equation with the nuclear recoil and QED corrections. Both corrections are obtained with the use of the conventional (Hermitian) DCB Hamiltonian. The nuclear recoil effect arising due to the finite nuclear mass M admits fully relativistic treatment only within the framework of QED [50,51]. Here we account for this effect in the lowest-order relativistic approximation and to first order in m_e/M via the inclusion of the mass shift operator [50,52]

$$H_{\rm MS} = \frac{1}{2M}\sum_{i,j}\left\{\mathbf{p}_i\cdot\mathbf{p}_j - \frac{\alpha Z}{r_i}\left[\boldsymbol{\alpha}_i + \frac{(\boldsymbol{\alpha}_i\cdot\mathbf{r}_i)\mathbf{r}_i}{r_i^2}\right]\cdot\mathbf{p}_j\right\} \quad (13)$$

into the DCB Hamiltonian. The nuclear recoil correction to the energy of the particular LL resonance is given by the first-order perturbation theory with respect to this additional term [42]. As already mentioned, in addition to the nuclear recoil corrections we supplement the complex rotated DCB energies with the QED corrections. The *ab initio* evaluation of these corrections still remains a challenging task even for He-like systems for which the methods of the QED calculations are currently well established (see, e.g., Refs. [53–55] and references therein). We thus compute the two-electron QED effects on the energies of the autoionizing states. In the present paper, we evaluate the QED corrections utilizing the model QED operator [56], constructed with the usage of the QEDMOD package [57]. We evaluate the QED correction as the difference between the CI results obtained with and without the model QED operator included into the DCB Hamiltonian. This approach has shown its efficiency in numerous investigations [38,39,49,58]. However, in the QED model operator method, the screened QED corrections are taken into account only approximately. These corrections as well as the QED part of the two-photon-exchange contributions give rise to another source of uncertainty. We also note that the frequency-dependent Breit correction was found to be of

TABLE IV. The comparison of the calculated energies E and Auger widths $\Gamma_{\rm Aug}$ of the LL resonances of the He-like ions with other nonrelativistic [60] and relativistic results [7]. All data are given in atomic units.

			This work		Other theory	
Z	Resonance	J	E	$\Gamma_{\rm Aug}$	E	$\Gamma_{\rm Aug}$
5	$2s^2_{1/2}$	0	−5.662 502(24)	$6.674(1)\times10^{-3}$	−5.66 088[a]	6.650×10^{-3}[a]
	$2p^2_{3/2}$	0	−5.145 465(42)	$3.0(2)\times10^{-4}$	−5.14 461[a]	3.010×10^{-4}[a]
	$2s_{1/2}2p_{1/2}$	0	−5.614 844(13)	$3.314(7)\times10^{-4}$	−5.612 99[a]	3.208×10^{-4}[a]
		1	−5.614 581(13)	$3.277(7)\times10^{-4}$		
	$2s_{1/2}2p_{3/2}$	2	−5.613 991(13)	$3.241(5)\times10^{-4}$		
6	$2s^2_{1/2}$	0	−8.291 878(40)	$6.944(1)\times10^{-3}$	−8.288 20[a]	6.910×10^{-3}[a]
	$2p^2_{3/2}$	0	−7.653 119(54)	$3.1(1)\times10^{-4}$	−7.651 06[a]	3.210×10^{-4}[a]
	$2s_{1/2}2p_{1/2}$	0	−8.234 485(22)	$3.377(6)\times10^{-4}$	−8.230 29[a]	3.220×10^{-4}[a]
					−8.234 485[b]	3.392×10^{-4}[b]
		1	−8.233 915(22)	$3.32(1)\times10^{-4}$	−8.233 914[b]	3.327×10^{-4}[b]
	$2s_{1/2}2p_{3/2}$	2	−8.232 652(22)	$3.27(1)\times10^{-4}$	−8.232 654[b]	3.269×10^{-4}[b]
7	$2s^2_{1/2}$	0	−11.422 672(64)	$7.146(1)\times10^{-3}$	−11.415 46[a]	7.100×10^{-3}[a]
	$2p^2_{3/2}$	0	−10.661 511(64)	$3.3(2)\times10^{-4}$	−10.657 32[a]	3.340×10^{-4}[a]
	$2s_{1/2}2p_{1/2}$	0	−11.355 781(34)	$3.444(2)\times10^{-4}$	−11.347 55[a]	3.230×10^{-4}[a]
		1	−11.354 691(34)	$3.363(6)\times10^{-4}$		
	$2s_{1/2}2p_{3/2}$	2	−11.352 301(34)	$3.289(5)\times10^{-4}$		
8	$2s^2_{1/2}$	0	−15.055 424(96)	$7.304(1)\times10^{-3}$	−15.042 66[a]	7.250×10^{-3}[a]
	$2p^2_{3/2}$	0	−14.171 026(76)	$3.4(2)\times10^{-4}$	−14.163 45[a]	3.440×10^{-4}[a]
	$2s_{1/2}2p_{1/2}$	0	−14.979 340(50)	$3.516(5)\times10^{-4}$	−14.964 81[a]	3.235×10^{-4}[a]
		1	−14.977 439(49)	$3.409(6)\times10^{-4}$		
	$2s_{1/2}2p_{3/2}$	2	−14.973 291(50)	$3.304(5)\times10^{-4}$		
9	$2s^2_{1/2}$	0	−19.190 81(14)	$7.434(3)\times10^{-3}$	−19.169 83[a]	7.365×10^{-3}[a]
	$2p^2_{3/2}$	0	−18.182 130(88)	$3.5(3)\times10^{-4}$	−18.169 51[a]	3.520×10^{-4}[a]
	$2s_{1/2}2p_{1/2}$	0	−19.105 923(70)	$3.600(7)\times10^{-4}$	−19.082 04[a]	3.240×10^{-4}[a]
		1	−19.102 832(70)	$3.463(7)\times10^{-4}$		
	$2s_{1/2}2p_{3/2}$	2	−19.096 092(70)	$3.326(8)\times10^{-4}$		
10	$2s^2_{1/2}$	0	−23.829 44(19)	$7.542(1)\times10^{-3}$	−23.796 99[a]	7.460×10^{-3}[a]
	$2p^2_{3/2}$	0	−22.695 19(10)	$3.6(2)\times10^{-4}$	−22.675 51[a]	3.585×10^{-4}[a]
	$2s_{1/2}2p_{1/2}$	0	−23.736 271(96)	$3.690(4)\times10^{-4}$	−23.699 27[a]	3.243×10^{-4}[a]
		1	−23.731 510(96)	$3.518(3)\times10^{-4}$		
	$2s_{1/2}2p_{3/2}$	2	−23.721 110(96)	$3.346(7)\times10^{-4}$		

[a]Ho [60].
[b]Müller *et al.* [7].

minor importance for the systems under investigation and, therefore, its contribution can be omitted.

Table III presents the energies and Auger widths of the LL resonances of the He-like ions from boron ($Z = 5$) to argon ($Z = 18$). In this table, the complex rotated DCB energy, the QED correction, and the nuclear recoil correction are shown explicitly. The presented Auger widths $\Gamma_{\rm Aug}$ were calculated only by means of the CS DCB Hamiltonian. The smallness of the Auger widths of the $2p^2_{1/2}$ ($J = 0$), $2p^2_{3/2}$ ($J = 2$), and $2p_{1/2}2p_{3/2}$ ($J = 1$) resonances is explained by the fact that the Auger decay of the $^3P_0$, $^3P_2$, and $^3P_1$ states corresponding to these resonances in the LS-coupling scheme, respectively, is strictly forbidden in the nonrelativistic limit. Indeed, due to parity and total angular-momentum conservation, the Auger decay is allowed only to the $1s\varepsilon s$ and $1s\varepsilon d$ configurations. In the nonrelativistic case, the transition to these configurations is forbidden by the conservation of the orbital angular momentum. Energies $E_{\rm tot}$ are supplemented with the total uncertainties from all calculated contributions as well as from uncalculated high-order QED corrections. The uncertainty due to the uncalculated QED corrections was estimated by analysis of the related contributions for the ground and single-excited states in He-like ions [53]. In most cases, the accuracy of the present calculations is limited by the uncertainties from the QED contributions. Using the presented results with the available high-precision data for the energies of the ground and lowest excited states (see Refs. [53–55]), one can easily find the corresponding transition energies.

In Table IV, we compare some of our results with other nonrelativistic [60] and relativistic calculations [7]. In Ref. [60], the calculations were performed by using the complex-scaling technique in combination with Hylleraas-type functions without taking into account the QED corrections. Since the nonrelativistic method cannot resolve the fine structure of the $2s2p$ resonance, for our three values for the $2s_{1/2}2p_{1/2}$ ($J = 0, 1$) and $2s_{1/2}2p_{3/2}$ ($J = 2$) states there is only one corresponding value from Ref. [60]. As one can see from the table, our results are in reasonable agreement with the nonrelativistic results. We also compared the values obtained for the carbon ion ($Z = 6$) with the recent relativistic calculations of Ref. [7]. These calculations were performed by employing the many-body perturbation theory in an all-order

formulation with the complex-scaling technique (see Ref. [30] and references therein). The QED corrections were taken into account by using the Welton method, which is different from the QED model operator approach. However, the results of Ref. [7] are in excellent agreement with our values.

IV. CONCLUSION

The energies and Auger widths of the *LL* resonances of the He-like ions from boron ($Z = 5$) to argon ($Z = 18$) have been evaluated by means of the complex-scaled configuration-interaction method. The systematic analysis of the uncertainty arising from the limited size of the configuration space was performed. The obtained energies have been compared with those calculated by using the stabilization and basic balancing methods. It was found that the energies obtained with these methods differ from the complex-scaling results by a shift that varies from about 1 to 10 meV.

The nuclear recoil and QED corrections were evaluated separately and added to the complex rotated Dirac-Coulomb-Breit energies. As the result, the most accurate theoretical predictions for the energies of the *LL* resonances are obtained. In most cases, the accuracy of the total results is limited by the uncertainties from the higher-order QED corrections.

ACKNOWLEDGMENT

This work was supported by the Russian Science Foundation (Grant No. 17-12-01097).

[1] P. Beiersdorfer, T. Phillips, V. L. Jacobs, K. W. Hill, M. Bitter, S. von Goeler, and S. M. Kahn, Astrophys. J. **409**, 846 (1993).

[2] K. Widmann, P. Beiersdorfer, V. Decaux, S. R. Elliott, D. Knapp, A. Osterheld, M. Bitter, and A. Smith, Rev. Sci. Instrum. **66**, 761 (1995).

[3] H.-J. Kunze, *Introduction to Plasma Spectroscopy*, Springer series on atomic, optical, and plasma physics (Springer-Verlag, Berlin, 2009).

[4] G. J. Tallents, *An Introduction to the Atomic and Radiation Physics of Plasmas* (Cambridge University Press, Cambridge, 2018).

[5] D. Porquet, J. Dubau, and N. Grosso, Space Sci. Rev. **157**, 103 (2010).

[6] A. C. Fabian and I. M. George, in *Iron Line Diagnostics in X-Ray Sources*, edited by A. Treves, G. C. Perola, and L. Stella (Springer-Verlag, Berlin, 1991), p. 169.

[7] A. Müller, E. Lindroth, S. Bari, A. Borovik, Jr., P.-M. Hillenbrand, K. Holste, P. Indelicato, A. L. D. Kilcoyne, S. Klumpp, M. Martins, J. Viefhaus, P. Wilhelm, and S. Schippers, Phys. Rev. A **98**, 033416 (2018).

[8] E. Balslev and J. M. Combes, Commun. Math. Phys. **22**, 280 (1971).

[9] J. Aguilar and J. M. Combes, Commun. Math. Phys. **22**, 269 (1971).

[10] R. A. Weder, J. Math. Phys. **15**, 20 (1974).

[11] R. A. Weder, J. Funct. Anal. **20**, 319 (1975).

[12] P. Seba, Lett. Math. Phys. **16**, 51 (1988).

[13] A. T. Kruppa, P.-H. Heenen, H. Flocard, and R. J. Liotta, Phys. Rev. Lett. **79**, 2217 (1997).

[14] S. Aoyama, T. Myo, K. Kato, and K. Ikeda, Prog. Theor. Phys. **116**, 1 (2006).

[15] K. Arai, Phys. Rev. C **74**, 064311 (2006).

[16] J.-Y. Guo, M. Yu, J. Wang, B.-M. Yao, and P. Jiao, Comput. Phys. Commun. **181**, 550 (2010).

[17] E. Lindroth, Phys. Rev. A **49**, 4473 (1994).

[18] E. Lindroth, Phys. Rev. A **52**, 2737 (1995).

[19] S. I. Themelis and C. A. Nicolaides, J. Phys. B: At., Mol. Opt. Phys. **28**, L379 (1995).

[20] N. Brandefelt and E. Lindroth, Phys. Rev. A **59**, 2691 (1999); **65**, 032503 (2002).

[21] G. Pestka, M. Bylicki, and J. Karwowski, J. Phys. B **39**, 2979 (2006); **40**, 2249 (2007).

[22] M. Bylicki, G. Pestka, and J. Karwowski, Phys. Rev. A **77**, 044501 (2008).

[23] S. B. Zhang and D. L. Yeager, Phys. Rev. A **85**, 032515 (2012).

[24] M. N. Medikeri and M. K. Mishra, Chem. Phys. Lett. **246**, 26 (1995); J. Chem. Phys. **103**, 676 (1995).

[25] S. Mahalakshmi, A. Venkatnathan, and M. K. Mishra, J. Chem. Phys. **115**, 4549 (2001).

[26] W. P. Reinhardt, Annu. Rev. Phys. Chem. **33**, 223 (1982).

[27] B. R. Junker, Adv. At. Mol. Phys. **18**, 207 (1982).

[28] Y. K. Ho, Phys. Rep. **99**, 1 (1983).

[29] N. Moiseyev, Phys. Rep. **302**, 211 (1998).

[30] E. Lindroth and L. Argenti, Adv. At. Mol. Opt. Phys. **63**, 247 (2012).

[31] B. Simon, Int. J. Quantum Chem. **14**, 529 (1978).

[32] E. Holøien and J. Midtdal, J. Chem. Phys. **45**, 2209 (1966); **45**, 3897 (1966).

[33] A. D. Isaacson and D. G. Truhlar, Chem. Phys. Lett. **110**, 130 (1984).

[34] R. Moccia and P. Spizzo, J. Phys. B: At. Mol. Phys. **20**, 1423 (1987).

[35] R. Lefebvre, J. Phys. B: At., Mol. Opt. Phys. **21**, L709 (1988).

[36] P. Froelich, M. Höghede, and S. A. Alexander, J. Chem. Phys. **91**, 1702 (1989).

[37] V. A. Mandelshtam, T. R. Ravuri, and H. S. Taylor, Phys. Rev. Lett. **70**, 1932 (1993).

[38] V. A. Yerokhin, A. Surzhykov, and A. Müller, Phys. Rev. A **96**, 042505 (2017); **96**, 069901(E) (2017).

[39] V. A. Yerokhin and A. Surzhykov, J. Phys. Chem. Ref. Data **47**, 023105 (2018).

[40] D. Andrae, Phys. Rep. **336**, 413 (2000).

[41] M. H. Chen, K. T. Cheng, W. R. Johnson, and J. Sapirstein, Phys. Rev. A **52**, 266 (1995).

[42] I. I. Tupitsyn, V. M. Shabaev, J. R. Crespo López-Urrutia, I. Draganić, R. S. Orts, and J. Ullrich, Phys. Rev. A **68**, 022511 (2003).

[43] D. A. Varshalovich, A. N. Moskalev, and V. K. Khersonskii, *Quantum Theory of Angular Momentum* (World Scientific, Singapore, 1988).

[44] V. M. Shabaev, I. I. Tupitsyn, V. A. Yerokhin, G. Plunien, and G. Soff, Phys. Rev. Lett. **93**, 130405 (2004).
[45] J. Sapirstein and W. R. Johnson, J. Phys. B: At., Mol. Opt. Phys. **29**, 5213 (1996).
[46] H. Bachau, E. Cormier, P. Decleva, J. E. Hansen, and F. Martín, Rep. Prog. Phys. **64**, 1815 (2001).
[47] B. Simon, Commun. Math. Phys. **27**, 1 (1972); Ann. Math. **97**, 247 (1973).
[48] V. A. Yerokhin and A. Surzhykov, Phys. Rev. A **86**, 042507 (2012).
[49] M. Y. Kaygorodov, Y. S. Kozhedub, I. I. Tupitsyn, A. V. Malyshev, D. A. Glazov, G. Plunien, and V. M. Shabaev, Phys. Rev. A **99**, 032505 (2019).
[50] V. M. Shabaev, Teor. Mat. Fiz. **63**, 394 (1985) [Theor. Math. Phys. **63**, 588 (1985)]; Yad. Fiz. **47**, 107 (1988) [Sov. J. Nucl. Phys. **47**, 69 (1988)]; Phys. Rev. A **57**, 59 (1998).
[51] G. S. Adkins, S. Morrison, and J. Sapirstein, Phys. Rev. A **76**, 042508 (2007).
[52] C. W. P. Palmer, J. Phys. B: At. Mol. Phys. **20**, 5987 (1987).
[53] A. N. Artemyev, V. M. Shabaev, V. A. Yerokhin, G. Plunien, and G. Soff, Phys. Rev. A **71**, 062104 (2005).
[54] V. A. Yerokhin and K. Pachucki, Phys. Rev. A **81**, 022507 (2010).
[55] A. V. Malyshev, Y. S. Kozhedub, D. A. Glazov, I. I. Tupitsyn, and V. M. Shabaev, Phys. Rev. A **99**, 010501(R) (2019).
[56] V. M. Shabaev, I. I. Tupitsyn, and V. A. Yerokhin, Phys. Rev. A **88**, 012513 (2013).
[57] V. M. Shabaev, I. I. Tupitsyn, and V. A. Yerokhin, Comput. Phys. Commun. **189**, 175 (2015); **223**, 69 (2018).
[58] I. I. Tupitsyn, M. G. Kozlov, M. S. Safronova, V. M. Shabaev, and V. A. Dzuba, Phys. Rev. Lett. **117**, 253001 (2016).
[59] I. Angeli and K. P. Marinova, At. Data Nucl. Data Tables **99**, 69 (2013).
[60] Y. K. Ho, Phys. Rev. A **23**, 2137 (1981).